THE JOURNAL OF PHYSICAL CHEMISTRY C

Article

pubs.acs.org/JPCC

Heterogeneous Charge Mobility in Individual Conjugated Polyelectrolyte Nanoparticles Revealed by Two-Color Single Particle Spectroelectrochemistry Studies

Robert Godin,[†] Rodrigo E. Palacios,[‡] and Gonzalo Cosa*,[†]

[†]Department of Chemistry and Center for Self-Assembled Chemical Structures (CSACS/CRMAA), McGill University, 801 Sherbrooke Street West, Montreal, QC H3A 0B8, Canada

[‡]Departamento de Química, Facultad de Ciencias Exactas Físico-Químicas y Naturales, Universidad Nacional de Río Cuarto, 5800 Río Cuarto, Córdoba, Argentina

Supporting Information

ABSTRACT: The optoelectronic properties of conjugated polymers and conjugated polyelectrolytes (CPEs) depend on their chain conformation and packing. Correlations between emission color, charge mobility, and extent of aggregation in these materials have been previously established from bulk studies. Here we describe the preparation of stable nanoparticle suspensions of the CPE poly[5-methoxy-2-(3-sulfopropoxy)-1,4-phenylenevinylene (MPS-PPV) where changes in the solvent composition enable tuning their emission spectra and quantum yield. By employing a newly developed color-sensitive single-molecule spectroelectrochemistry (SMS-EC) technique, the effect of chain conformation on the optoelectronic properties of MPS-PPV nanoparticles is monitored at the single particle level. Within a single particle the photoluminescence and redox response is chromatically correlated reflecting on the differing contributions that coiled and deaggregated vs extended and packed segments have on their optoelectronic properties. We also observe a heterogeneous response among nanoparticles to externally applied electrochemical potentials, which further correlates with their emission color (chain packing). We rationalize our observations on differential charge injection, energy and charge transport, and ion migration as a consequence of chain conformation, packing effects, and the presence of electrochemically reducible quenching sites. Our work provides a way to unravel the intrinsic heterogeneity of CPE materials to better understand the relationship between chain conformation and optoelectronic properties.

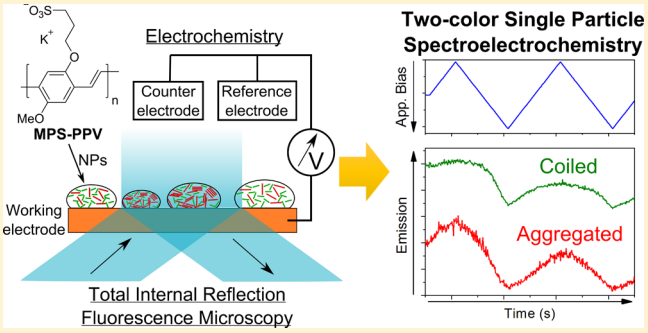

INTRODUCTION

Conjugated polymers and conjugated polyelectrolytes (CPEs)[1] have become customary building blocks for optoelectronic devices such as LEDs, thin-film transistors, chemical sensors, and photovoltaics.[2−8] Their increasing importance in the manufacturing industry arises from both their ease of processability and tunable electronic and optical properties. These properties are intimately related to the conformation of individual chains along the polymer backbone and to the distance between chains.[9−14] In this context, increased charge carrier mobilities, reduced emission quantum yield, red-shifted emission spectrum, and increased exciton transport properties have been observed experimentally as a result of the increase of conjugation length caused by extension of the polymer backbone as well as by the formation of interchain species.[15−21]

Given the amphiphilic nature of CPEs (hydrophobic backbone with π-delocalized electronic structure and repeat units that bear pendant substituents with ionic functionalities),[1] their chain conformation and extent of aggregation in solution may be tuned upon careful solvent choice.[22−25] CPEs provide in this regard unique systems to explore how the interplay of chain conformation and aggregation affect electronic and optical properties at the nanoscale.

Here we show that adjusting the water content in water/tetrahydrofuran (H_2O/THF) and water/acetonitrile (H_2O/MeCN) mixtures enables control of the chain conformation and aggregation of the conjugated polyelectrolyte poly[5-methoxy-2-(3-sulfopropoxy)-1,4-phenylenevinylene] (MPS-PPV, see Figure 1). Conjugated polyelectrolyte nanoparticles (NPs) with emission spectra peaking in the range from ca. 620 to 545 nm and with up to 46-fold increase in relative emission intensity are readily obtained upon careful selection of the solution conditions.

We also show that the effect of chain conformation on the optical and electronic properties of MPS-PPV can be monitored at the single nanoparticle level with the aid of a

Received: April 10, 2015
Revised: May 18, 2015
Published: May 19, 2015

DOI: 10.1021/acs.jpcc.5b03491
J. Phys. Chem. C 2015, 119, 12875−12886

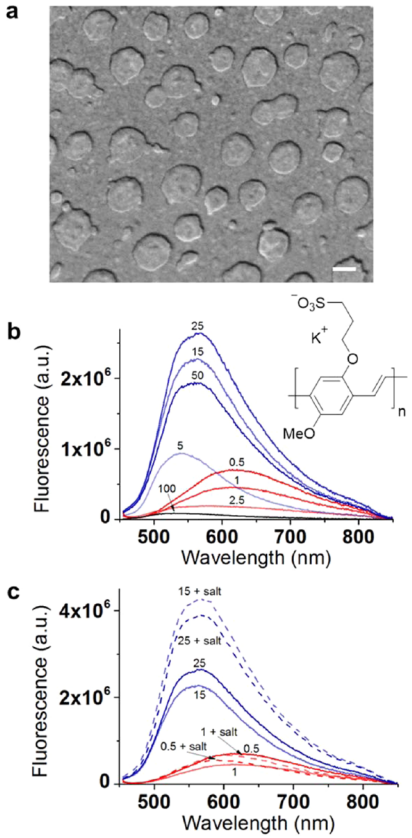

Figure 1. (a) SEM image of MPS-PPV NPs (formed in 0.5% H_2O v/v in THF solution) dispersed on a glass coverslip. See sample preparation details in the text. Scale bar is 100 nm. Fluorescence emission properties of MPS-PPV dispersed in various H_2O/THF solutions (b) before (solid lines) and (c) after (dashed lines) addition of 100 mM Bu_4NClO_4 as a powder, λ_{ex} = 450 nm in both cases. Panel (c) also shows spectra of two samples before addition of Bu_4NClO_4 (solid lines) to allow for direct comparison. The water content (in % v/v) is indicated near the fluorescence maximum in each trace. The low water regime (≤2.5% H_2O by volume) is shown in red while the high water regime (≥5% H_2O by volume) is shown in blue. Fluorescence in water-only solution is shown in black. Shown in the inset is the chemical structure of MPS-PPV.

novel color-sensitive single-molecule spectroelectrochemistry (SMS-EC) technique. This technique enabled recording the distribution of the potentials required to inject charges (both from the ground state and photoexcited states) for individual CPE NPs, offering new information on the heterogeneity of the redox process of CPEs at the molecular level. The simultaneous monitoring of the red (extended/aggregated polymer backbone) and green (coiled and deaggregated backbone) emission components as a function of applied bias in an electrochemical cell configuration allowed us to unearth the interplay between charge injection (thermal and photoinduced), energy transfer, and photoluminescence in individual MPS-PPV NPs and correlate them to CPE conformation.[26] We demonstrate that NPs of MPS-PPV display differing emissive behavior when subjected to an externally applied electrochemical bias. This is manifested in both the response speed and modulation amplitude exhibited between different nanoparticles. Within a single particle the photoluminescence response is also chromatically correlated reflecting on the differing contributions that coiled and deaggregated vs extended and packed segments have on the optoelectronic properties.

Our studies provide a method that distinguishes between individual MPS-PPV NPs with lower or higher charge mobility, caused by chain packing effects, for example, and thus make it possible to evaluate the effectiveness of various approaches aimed at modifying chain conformation for specific applications. Our work provides a way to unravel the intrinsic heterogeneity of CPE materials to better understand the relationship between chain conformation and optoelectronic properties.

EXPERIMENTAL SECTION

Preparation of MPS-PPV Solution in H_2O/Organic Solvent for Ensemble Measurements. An initial MPS-PPV stock solution (0.25% w/w in H_2O, 9.5 mM in polymer repeat units) was centrifuged for 5 min at 5000 rpm on a benchtop centrifuge (accuSPIN micro, Fisher Scientific) to precipitate large aggregates. In order to prepare the various H_2O/organic solvent dispersions, 10 μL aliquots of the supernatant were brought to a final desired H_2O volume before adding to the organic solvent in order to complete 2 mL of H_2O:organic solution with the desired % v/v H_2O content. To ensure reproducibility, the aqueous MPS-PPV solution thus obtained was diluted at most 10× in the water-miscible solvents THF or MeCN by rapid injection, and next the resulting solution was added to the remaining organic solvent to complete 2 mL. For H_2O volumes >200 μL, a single injection was performed into the organic solvent to yield a final volume of 2 mL. The MPS-PPV stock was thus diluted 200-fold in all ensemble experiments yielding a final polymer repeat unit concentration of 48 μM.

Ensemble Spectroscopy. Fluorescence measurements were performed on a PTI Quantamaster 40 fluorimeter at 25 °C with excitation at 450 nm. UV−vis spectra were obtained at room temperature (23 ± 1 °C) on a Hitachi U-2800 spectrophotometer. DLS measurements were performed on a Brookhaven Instruments NanoBrook 90Plus at 90° detection angle, 25 °C with nominally 640 nm laser light.

SEM Imaging. Coverslips were cleaned by immersing them for 1 h in a piranha solution (30% H_2O_2 and H_2SO_4 1:3 v:v). They were next thoroughly rinsed with H_2O and EtOH. MPS-PPV NPs (0.5% v/v H_2O content) were spin-coated by dropping 40 μL of solution on the clean coverslips rotating at 3000 rpm. The spinning was then slowed to 2000 rpm and kept for 50 s afterward. A thin gold coating (~10 nm) was then argon-sputtered in a vacuum environment to give sufficient sample conductivity. The SEM images were acquired on a FEI Inspect F-50 FEG-SEM operating at 10−20 kV in backscatter detection mode.

Single Molecule Spectroelectrochemistry. MPS-PPV NPs (0.5% v/v H_2O content in THF) were spin-coated by dropping 40 μL of solution on a clean ITO-coated coverslip (Evaporated Coatings Inc., 50 Ω/□; cleaned by 20 min sequential sonication in acetone, trichloroethylene, and methanol) rotating at 3000 rpm. The spinning was then slowed to 2000 rpm and kept for 50 s. A glass tube was affixed on top of the coverslip with the help of epoxy glue (Hardman, McMaster-Carr). The epoxy was cured in an oven (110 °C) for ca. 1 h, which also dried the sample. The solvent utilized was MeCN and the supporting electrolyte was Bu_4NClO_4 (0.1 M). The electrochemical cell was completed by sealing with an inverted septum, which was pierced by a nonaqueous Ag/Ag^+ reference electrode and Pt wire counter electrode. The ITO surface served as the working electrode and four ITO sectors

DOI: 10.1021/acs.jpcc.5b03491
J. Phys. Chem. C 2015, 119, 12875−12886

Table 1. Spectroscopic and DLS Characterization of MPS-PPV Dispersions in H_2O/THF Solutions

		MPS-PPV + H_2O + THF			MPS-PPV + H_2O + THF + Bu_4NClO_4		
H_2O[a] (%v/v)	n_{H2O}/n_{THF}	λ_{em}[b] (nm)	diameter[c] (nm)	relative emission[b]	λ_{em}[b] (nm)	diameter[c] (nm)	relative emission[b]
0.5	0.02	622	212	9	588	1900	7
1.0	0.05	613	146	6	605	3300	8
2.5	0.12	583	110	3	544	1360	18
5.0	0.24	543	82	9	566	1494	36
15	0.79	557	N/D	24	570	N/D	46
25	1.50	568	N/D	28	571	N/D	42
50	4.50	559	N/D	21	N/A	N/A	N/A
100	-	518	N/D	1	554	N/D	4[d]

[a]In THF. [b]Wavelength corresponding to the maximum of the emission spectrum. The excitation wavelength utilized was 450 nm, and absorption at this wavelength did not vary more than ~10%. Emissions intensities are relative to the emission of MPS-PPV in pure water. Absorption and emission intensities of solutions containing particles larger than ~300 nm are likely to be affected by the penetration depth of light into the CPE.[31] [c]As measured by DLS. [d]Saturated solution of Bu_4NClO_4 in H_2O (concentration ≪100 mM). N/D = not detectable.

on the coverslip could be addressed independently. The cell was degassed for at least 1 h with Ar before measurements. An argon-filled balloon was affixed to the sample at all times to ensur an Ar positive pressure within the electrochemical cell. Individual MPS-PPV NPs were imaged using a wide-field objective-based total internal reflection fluorescence (TIRF) microscopy setup consisting of an inverted microscope (IX71, Olympus) equipped with a laser-based TIRF illumination module (IX2-RFAEVA-2, Olympus). Samples were excited with the evanescence wave of a 488 nm Ar^+ laser output (Melles Griot), obtained by focusing the collimated laser beam at back focal plane of a high numerical aperture (N.A. = 1.45) oil-immersion objective (Olympus PLAN APO 60×) and launching the excitation past the critical angle. The laser power measured at the exit of the objective was 970 μW. Emission was collected through the same objective and images were magnified 2-fold via a lens system and then captured on a back illuminated electron multiplying charge coupled device (EM-CCD) camera (Cascade II:512B, Roper Scientific). Images were spectrally separated by a 640dcxr dichroic mirror to give two distinct emission channels, a green channel with λ_{em} < 640 nm, and a red channel with λ_{em} > 640 nm. A total area of about 66 × 33 μm^2 was imaged at any given time. The images were analyzed with custom Matlab and IDL scripts that identified diffraction-limited fluorescence spots, registered them in both spectral channels and calculated the background-corrected integrated fluorescence intensity for each individual NP in either the green or red channel. Electrochemical potential was controlled by a CHI600D electrochemical analyzer. The applied bias (E_{app}) and acquired movies were temporally synchronized. The reference electrode was calibrated with ferrocene ($E^0_{Fc+/Fc}$ = 0.64 V vs NHE) at the end of the experiment. Potentials indicated are vs NHE. A cyclic voltammetry potential waveform was applied to the sample, the E_{app} were initiated at +0.53 V and were first swept to the minimum peak potential (either +0.03 V (Figure 2) or −0.97 V (Figure 5)) and then to the maximum peak potential of +1.03 V. Potentials were scanned at a rate of either 50 or 100 mV/s, while frames were acquired at a rate of 10 Hz.

RESULTS AND DISCUSSION

Effect of Water Content in H_2O/THF and H_2O/MeCN Mixtures. We prepared CPE NPs by rapidly injecting a CPE aqueous solution into the water-miscible organic solvent, either THF or MeCN. During injection, individual MPS-PPV chains aggregate or collapse to form CPE NPs. This nanoprecipitation process is analogous (albeit with opposite polymer and solvent polarities) to the method reported to produce neutral conjugated polymer NPs following injection of their THF solutions into H_2O.[27] This reprecipitation method has been extensively used to form conjugated polymer NPs, but is far less common for the case of conjugated polyelectrolytes.[28−30] Nanoparticle formation was monitored via dynamic light scattering (DLS) analysis of dispersions of MPS-PPV in various H_2O/THF and H_2O/MeCN mixtures, ranging from 0.5% to 100% v/v in water (see Table 1 and Table S1). Nanoparticles of MPS-PPV 212 nm in diameter (by DLS) were recorded at 0.5% H_2O/THF v/v. These NPs were also observed in scanning electron microscopy (SEM) micrographs, although we recorded a smaller average size of 124 nm in diameter (Figures 1 and S1). The difference in size presumably arises due to swelling of the NPs in solution for the DLS experiments. Increasing the water content above 0.5% v/v led to a reduction of the recorded size of the NPs in our DLS studies as better solubilization of the CPEs takes place. At water contents above 15% v/v, the scattering counts were below the detection limit of our setup.

The chain conformation of CPEs was extremely sensitive to nanoparticle preparation conditions. We observed a broad, red-shifted fluorescence at very low water content in water/THF solutions, in the range of 0.5−2.5% H_2O v/v (see Table 1 and Figure 1). At higher water contents (5−50% H_2O v/v) the fluorescence intensity was significantly enhanced (up to 10-fold increase) and the emission spectrum, while still broad, was markedly blue-shifted (up to 80 nm). Similar trends were observed for MPS-PPV dispersed in H_2O/MeCN solutions; however, the fluorescence enhancements were not nearly as pronounced as those in THF presumably because MeCN is a poor solvent for the PPV backbone (see Figure S2). Changes in absorption spectra with increasing H_2O content were also consistent with conformational changes. A decreasing proportion of red-absorbing sites were recorded in going from 0.5% to 50% H_2O by volume in THF (see Figure S3). At the lowest water content, broadening of the absorption peak, indicative of a large distribution of conjugation lengths and/or chain conformations, was observed. Also recorded was a red-absorbing tail which extended up to ~600 nm.

Although it is difficult to assign the red fluorescence to a specific emitting species,[32] the fact that red-absorbing sites are formed in our system (see Figure S3) indicates an increase in the average conjugation length and/or the formation of aggregates. While more specific assignment of the red-emitting

DOI: 10.1021/acs.jpcc.5b03491
J. Phys. Chem. C 2015, 119, 12875−12886

species is beyond the scope of the present study, it is important to recall that the origin of red-shifted fluorescence in conjugated polymers has been previously attributed to an increase in the conjugation length and/or to the formation of interchain species.[33−38] Here, "interchain species" denotes a group of non-neighboring chromophore segments in the polymer backbone that are in contact.[18,39] Following the nomenclature defined by Schwartz,[18] the term "aggregates" refer to interchain species that interact in the ground state. Excimers in turn refers to interchain species that interact exclusively in the excited state, resulting in changes in the fluorescence, but not the absorption spectra.[40]

Insight on the CPE chain conformation can be gained by comparing the observed spectral and NP size trends (Table 1). Increasing the water content from 0.5% to 15% v/v leads to smaller NPs with blue-shifted fluorescence. With increasing water content the CPE becomes relatively well solvated and interchain interactions between MPS-PPV chains are less prominent, leading to a blue-shift in the absorption and fluorescence spectra and a marked increase in emission intensity. Similar observations have been made with MPS-PPV dispersed in mixtures of H_2O and DMSO (a good solvent for MPS-PPV chains), where a large fluorescence enhancement in pure DMSO was recorded and assigned to the absence of exciton−exciton annihilation within the PPV backbone.[41] We postulate that, at very low water content, MPS-PPV chain segments are straightened out and bury the charged side groups within water-rich pools, effectively increasing the average conjugation length of the chromophores.[18] In turn, the extended conformation allows for better $\pi-\pi$ stacking between chromophores promoting the formation of interchain species (aggregates and excimers) and NPs. Increased interchain interactions lead to red-shifted (and weak) fluorescence as low-energy emissive sites (and nonemissive sites) are eventually populated upon extensive energy transfer.[42−44]

We next explored the role that the large hydrophobic counterion tetrabutylammonium perchlorate (Bu_4NClO_4) has on the spectroscopic properties of MPS-PPV (Figure 1c). The information is relevant to our single molecule/particle spectroelectrochemistry studies where Bu_4NClO_4 was used as the supporting electrolyte (vide infra). In the presence of Bu_4NClO_4, we observed a significant increase in fluorescence when MPS-PPV was dispersed in 15% H_2O v/v in THF. A maximal 46-fold fluorescence enhancement was observed compared to MPS-PPV dispersed in neat H_2O with no Bu_4NClO_4. These observed changes in luminescence, also recorded in H_2O/MeCN solutions, point to better solvation of MPS-PPV polymer chains when an organic cation is added to a H_2O/organic solvent mixture rich in the organic fraction. The alkyl groups in the large counterion act as spacers that effectively separate polymer chains and inhibit their contact.[45] The greasy counterions may additionally minimize the tendency of CPEs toward packing with each other to reduce contact with water, exerting a surfactant effect. At water contents of 1% or lower, the emission enhancement of MPS-PPV was significantly smaller, indicating that Bu_4NClO_4 did not significantly alter the NPs structure under these conditions. A similar effect is expected under the anhydrous conditions we employed in our single molecule measurements described below.

Single Molecule Spectroelectrochemistry of MPS-PPV Particles. In order to unravel the role that chain conformation plays in the differential optoelectronic behavior of individual MPS-PPV NPs we developed a two-color single-molecule spectroelectrochemistry (SMS-EC) technique to correlate changes in either green (coiled/deaggregated) or red (extended/aggregated) emission with applied electrochemical bias (E_{app}).[46] Specifically, NPs were spin-cast onto an ITO coated glass coverslip (working electrode) and an airtight electrochemical cell was assembled with reference and counter electrodes (Figure 2a). Samples were next mounted on a total internal reflection fluorescence microscope (TIRFM). Images were recorded at 10 Hz rate in an electron multiplied CCD camera (EMCCD) while sweeping the external potential E_{app} in the electrochemical cell. Tens of surface immobilized NPs could thus be followed over time. Intensity vs time trajectories for each individual particle in both color channels were constructed from the stack of images (Figure 2b). We studied NPs formed in 0.5% v/v H_2O in THF as the solution properties

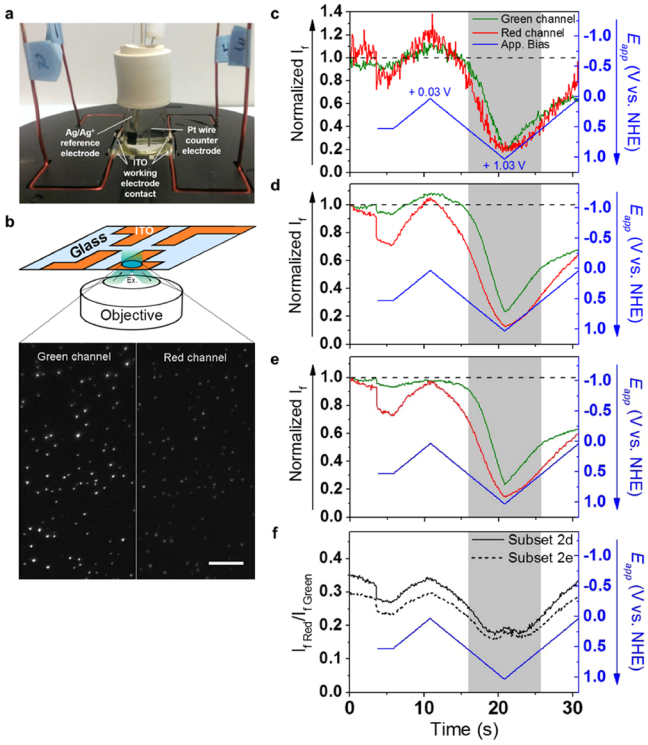

Figure 2. Effect of applied bias on MPS-PPV NP fluorescence as measured by TIRFM based color-sensitive SMS-EC. (a) Photograph of the SMS-EC cell. (b) Cartoon illustrating the coverslip with four independent ITO working electrodes and the evanescent optical excitation. The resulting emission from individual nanoparticles is collected by the objective and relayed to the chip of an EM CCD camera for image capture. One acquired frame is shown below depicting real data in the green and red channels. The scale bar is 10 μm. (c) Chromatically resolved (green and red) SMS-EC single particle fluorescence intensity trajectories normalized to the initial fluorescence intensities. Panels (d) (47% of the total) and (e) (53% of the total) show normalized ensemble fluorescence intensity trajectories for two subsets of NPs showing differing enhancement behavior in the green channel under E_{app} in the region between +0.03 V and +0.54 V. Dashed lines corresponding to the initial intensities are visual guides to emphasize the changes in intensity. (f) Non-normalized red-to-green fluorescence intensity ratios for NP subsets presented in (d) and (e). Peaks seen at E_{app} near +1 V are artifacts resulting from the fluorescence intensity in the red channel dropping near background levels. A total of 68 NPs were analyzed. Time intervals where E_{app} was > +0.54 V are highlighted in gray.

DOI: 10.1021/acs.jpcc.5b03491
J. Phys. Chem. C 2015, 119, 12875−12886

of these NPs, characterized by a high level of interchain interactions, are expected to be representative of those corresponding to NPs deposited on a surface and monitored in dry MeCN solutions.

In the following we first describe our results for a "narrow" E_{app} range (+0.03 to +1.03 V vs NHE, Figure 2) and discuss the phenomena occurring in this E_{app} range (thermal electrochemical oxidation and photoinduced electron transfer). Results obtained for a wider E_{app} range, keeping the maximum at +1.03 V but extending on the reductive side to −0.97 V (Figure 5), are next presented and the new processes occurring (asymmetric fluorescence enhancement and differences in hole filling) are discussed in the context of polymer morphology.

Results for +1.03 V ≥ E_{app} ≥ +0.03 V. Shown in Figure 2 are representative normalized fluorescence intensity trajectories for a single particle and subensembles (average of selected single particle trajectories), recorded in both the green and red channels upon scanning the E_{app} linearly over time between +0.03 V and +1.03 V vs NHE (see Figure S4, for non-normalized intensities). Starting with an open circuit, applying a potential of +0.53 V (at time = 4 s) resulted in a slight reduction of fluorescence intensity (I_f) in the green channel, yet a marked one in the red channel. As E_{app} was swept toward 0 V (up to time = 11 s), all particles showed a reversible I_f enhancement in the red channel. For the green channel a subset of particles (ca. 50%) showed I_f enhancements, albeit smaller in relative magnitude to those observed in the red channel (Figure 2d). The changes in I_f are reversed as the bias is swept linearly over time from +0.03 V back to +0.53 V (from 11 to 16 s). In contrast, the remaining particles showed negligible changes in I_f (Figure 2e).

At the onset E_{app} of ∼ +0.54 V and increasing until +1.03 V, a sharp quenching of the fluorescence intensity was observed followed by a steady recovery upon scanning E_{app} back from +1.03 V to +0.54 V (gray regions in Figure 2, corresponding to potentials ≥ +0.54 V). The quenching and recovery in this bias range were equally prominent in both the green and red channels. However, for both channels, the intensity did not fully recover at the end of the first cycle. This is probably the result of either permanent photodamage to the polymer or irreversible reactions taking place after extensive electrochemical oxidation of MPS-PPV.[47] Similar conclusions applied to I_f trajectories recorded during a second potential applied immediately following the first cycle (see Figures S5 and S6).

The marked I_f quenching observed as E_{app} is swept above the +0.54 V onset potential and the recovery recorded in the return sweep are consistent with the reversible electrochemical oxidation of the ground state of MPS-PPV. Exciton quenching has been observed in similar studies conducted on MEH-PPV, the nonionic counterpart of MPS-PPV, upon hole injection and formation of a radical cation.[48] The onset p-doping potentials of other 2,5-dialkoxy-substituted PPVs have been reported to be in the range of +0.85 to +0.91 V vs NHE,[49,50] consistent with our assignment of oxidation of MPS-PPV NPs at potentials more positive than +0.54 V (see discussion below for $E_{1/2}$ values) and indicative of the high sensitivity of photoluminescence intensity to the presence of holes (radical cation species) in this CPE. Alternatively, electric field-induced fluorescence quenching has been observed for conjugated polymer chains.[51−53] We do not expect our data to be significantly affected by electric-field effects since the electric field generated at the electrode/solution interface is suppressed at distances beyond 1 nm (the extent of the electrochemical double layer) by the high concentration of supporting electrolyte. The charges present in MPS-PPV would also result in screening of the electric field within the NPs. It is possible that the emitting sites located at the interface of the electrode exhibit electric field-induced quenching, although these are presumed to be a small fraction of the total emitting sites of the NPs. Most importantly, the polarity of the applied bias influences the fluorescence changes and is inconsistent with a purely electric field-driven process.

Importantly, the distribution of potentials at which I_f is quenched by half relative to the initial I_f ($E_{1/2}$) and the I_f modulation depth we recorded were very similar for all particles in both color channels. The $E_{1/2}$ for each particle and for both color channels was very narrow, ca. ±0.03 V. The mean $E_{1/2}$ recorded in the red channel, ∼ +0.8 V, was slightly smaller than that recorded for the green one, ∼ +0.9 V (see Figure 3). The smaller value of $E_{1/2}$ recorded in the red vs green channel, while initially surprising, is readily rationalized considering that segments with an average longer conjugation (red-emitting sites) are easier to oxidize than those with shorter conjugation (green-emitting sites).[54] As the values of $E_{1/2}$ relate to the ground state oxidation process,[48] we conclude that a significant

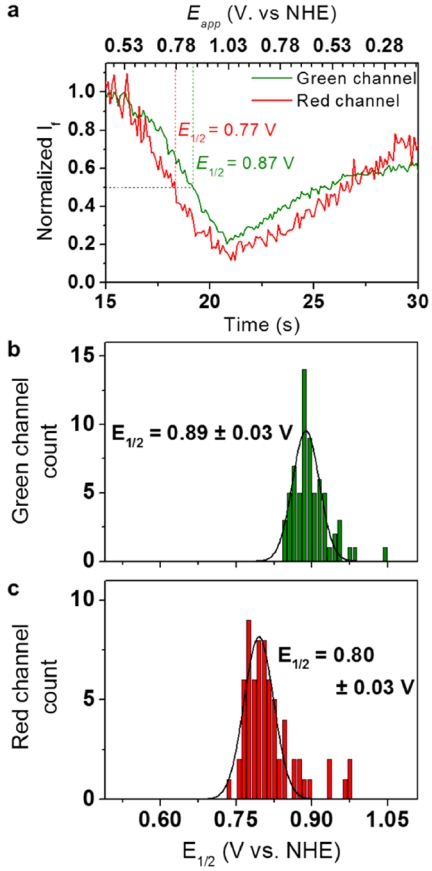

Figure 3. Distributions of $E_{1/2}$ values determined from single particle intensity-time trajectories. (a) Representative chromatically resolved (green and red) single particle fluorescence intensity trajectories recorded in our two-color SMS-EC setup. The I_f recorded at +0.54 V, before the first oxidative quenching event, was taken to be 1. The $E_{1/2}$ is the applied bias where the intensity dropped by half. The center and width of the Gaussian distributions were taken to represent the mean and the standard deviation of $E_{1/2}$ values. Panels (b) and (c) display data extracted from the green and red channels for both NP subsets shown in Figure 2d and e.

DOI: 10.1021/acs.jpcc.5b03491
J. Phys. Chem. C 2015, 119, 12875−12886

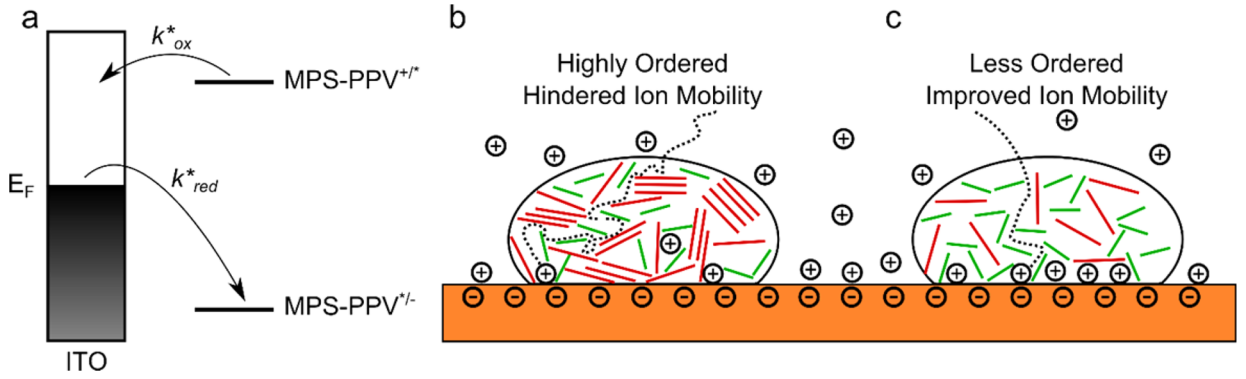

Figure 4. Cartoons illustrating: (a) State energy diagram for the MPS-PPV/ITO system. In SMS-EC experiments the energy of the ITO Fermi level (E_F) is modulated by an external bias. (b,c) Hypothetical ordering of MPS-PPV NPs on an ITO electrode, where the polymer backbone is either (b) extended and aggregated or (c) coiled and deaggregated.

portion of the red-emitting sites are present in the ground state (i.e., they are not excimers). This is in line with the observation of red-absorbing sites in the MPS-PPV NPs (Figure S3).

The I_f modulation depth we recorded was ca. 80% (75% in the green channel, 85% in the red channel) relative to the initial I_f. The narrow distribution of $E_{1/2}$ along with the observation that all particles showed high I_f modulation depth indicate that all the studied particles were in good ohmic contact with the ITO working electrode.[26,48] The observation that the quenching modulation depth was ~80% within a relatively narrow 0.5 V bias range above the quenching onset indicates that holes injected in these NPs were significantly electrostatically screened from each other, presumably by the sulfonate side groups along the polymer backbone. This screening permitted the efficient injection of multiple holes necessary to account for the large modulation depth in a ca. 100-nm-diameter nanoparticle, within the short bias range experimentally recorded. The large fluorescence intensity modulation in the short bias range compares to the results recorded with small (25 nm diameter) NPs of MEH-PPV, where 98% fluorescence quenching was achieved within a 0.3 V range.[48] Solvent penetration and external ion screening were called upon to justify the narrow range and large modulation with MEH-PPV small particles. These factors would also be operational in the ionic MPS-PPV.

Having unraveled the origin of the fluorescence intensity quenching at $E_{app} \geq +0.54$ V as thermal hole injection, we next discuss the observed modulation in I_f for E_{app} between +0.54 V and +0.03 V (white regions of Figure 2c–f). Specifically, we address first the origin of the I_f enhancement with reduction in E_{app}, and next the particle-to-particle heterogeneous behavior observed for the green channel and the differential relative amplitude of I_f for the two channels (green vs red).

Excited state electrochemical oxidation and reduction processes (photoinduced electron transfer (PeT) from (to) photoexcited MPS-PPV to (from) ITO) are both plausible in the potential range between +0.54 V and +0.03 V, resulting in the quenching of polymer emission. In turn, no ground state redox process is known to occur for MPS-PPV in this bias range. We thus assigned the observed voltage-induced intensity modulation in the above potential range to changes in the rate of photoinduced redox processes from photoexcited MPS-PPV (see Figure 4). Lowering E_{app} (raising the Fermi level (E_F) of ITO) should decrease the rate constant for photoinduced oxidation (k^*_{ox}) concomitant with a reduction in the driving force for the oxidation of MPS-PPV. In turn, the rate constant for photoinduced reduction (k^*_{red}) should increase as E_{app} is lowered. Considering the initial segment of the intensity–time trajectories, engaging the bias at +0.53 V (Figure 2c–e, time = 4 s) leads to a drop in the I_f of the nanoparticles compared to the open circuit case. This is consistent with an overall increase in the PeT rate (sum of k^*_{ox} and k^*_{red}, Figure 4). Subsequent lowering of the bias enhanced the I_f, in line with a relatively smaller increase of k^*_{red} compared to the decrease of k^*_{ox} under these conditions. The observation that a nanoparticle I_f recorded under applied bias may surpass the I_f recorded at open circuit further signals that PeT was already operational at open circuit, resulting in static quenching of the polymer emission.[48]

It is interesting to note that different results were obtained for the modulation of I_f with E_{app} for charged vs uncharged conjugated polyphenylene vinylene (PPV) polymers in the bias range between 0 V and +0.54 V. These discrepancies underscore the role of side groups in tuning the photophysical properties of the PPV parent backbone. Specifically, previous SMS-EC studies conducted on MEH-PPV NPs showed a linear modulation of I_f with E_{app} under mild electrochemical potentials.[48] The results however showed a drop in intensity with decreasing E_{app}, contrary to our results with MPS-PPV. With MEH-PPV it was concluded that excited state reduction of the polymer chains was the dominant pathway, i.e., with decreasing bias (raising the E_F of ITO) the increase in k^*_{red} and ensuing quenching is more important than the drop in k^*_{ox} that would lead to enhanced I_f. Our studies with MPS-PPV are in line with excited state oxidation being the dominant process at play in this bias range. The change of regime from overall photoinduced reduction (MEH-PPV) to overall photoinduced oxidation (MPS-PPV) is possibly related to the lowering of the barrier to electron injection into ITO due to the dipole created at the ITO surface from negatively charged side groups on MPS-PPV.[55−57]

Following our discussion on thermal and photoinduced redox processes accounting for the modulation of I_f in the bias range between 0 V and +1 V, we next address the particle-to-particle heterogeneous behavior observed for the green channel and the differential relative amplitude of I_f for the two channels (green vs red) (see Figure 2). These experimental observations may be rationalized by considering the effects of ion motion through the MPS-PPV NPs and the extent of aggregation and energy transfer characterizing green and red emissive sites as described in detail below. Briefly, the rearrangement of ions that occurs when a potential is applied results in the formation

DOI: 10.1021/acs.jpcc.5b03491
J. Phys. Chem. C 2015, 119, 12875−12886

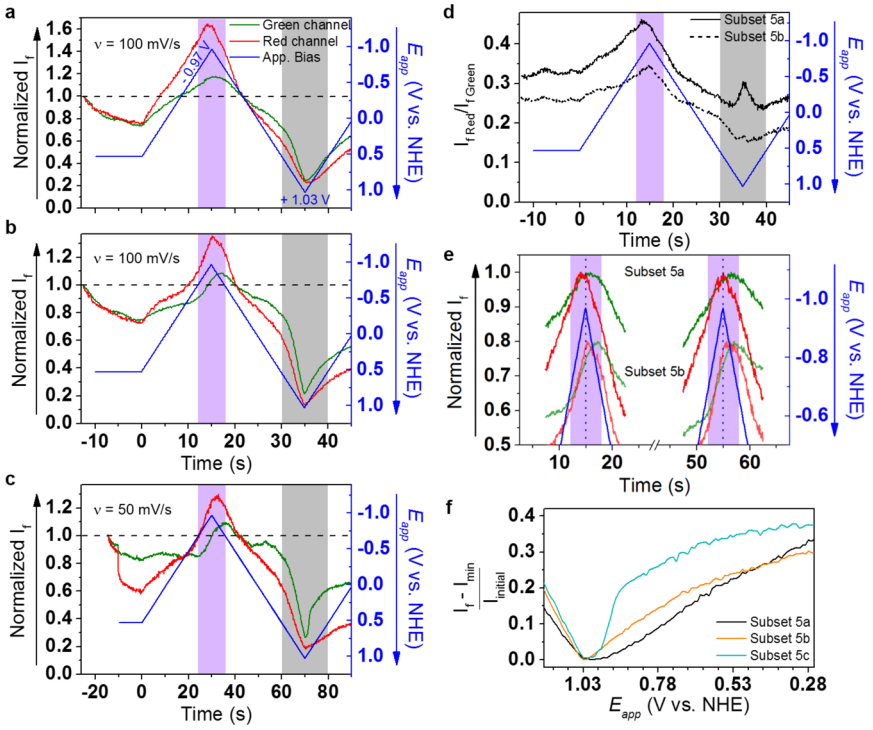

Figure 5. MPS-PPV NP fluorescence as measured by two-color SMS-EC showing the effect of negative applied biases ($-0.97 \leq E_{app} \leq +1.03$ V). (a,b) Average time trajectories normalized to the initial intensities of two subsets of NPs imaged in the same experiment and showing differing behavior at a potential scan rate of 100 mV/s. (a) NPs where I_f is highly sensitive to changes in E_{app}. (b) NPs that show an asymmetric I_f enhancement at an onset of ~ −0.68 V. (c) Results for MPS-PPV NPs when the potential scan rate is reduced to 50 mV/s, normalized to the initial intensities. Only one type of NP behavior is seen (n = 37 particles). (d) Non-normalized red-to-green fluorescence intensity ratios for NP subsets presented in (a) and (b). Peaks seen at E_{app} near +1 V are artifacts resulting from the fluorescence intensity in the red channel dropping near background levels. (e) Changes in normalized fluorescence intensity relative to the maximum I_f for the NP subsets shown in (a) and (b). The traces of subset 5b are offset by 0.2 units to increase clarity. (e) Changes in normalized fluorescence relative to the minimum I_f recorded in the green channels at the first positive peak potential for NP subsets shown in (a), (b), and (c). Data shown corresponds to time = 25−45 s for subsets 5a and 5b, and time = 50−70 s for subset 5c. Time intervals where E_{app} is > +0.54 V are highlighted in gray, while those where E_{app} is < −0.68 V are highlighted in purple.

of a double layer and changes of the electric field in the vicinity of the electrode.[58] The resulting reorganization affects the kinetics of photoinduced redox processes between ITO and MPS-PPV.

We postulate that the ease of external ion migration through the NPs will dictate the sensitivity of I_f to E_{app} in a potential window where the only mechanism that modulates I_f is PeT. Higher external ion mobility and easier chain reorganization should lead to better screening of the electric field generated at the working electrode and a lower sensitivity of I_f to changes in potential. We note that the indistinguishable ground state oxidative quenching behavior recorded for the subset of NPs in Figure 2d and e (see also Figure S9b) is consistent with similar polymer chain interactions in both systems, including charge transport characteristics. In this regard, the differential behavior between subsets in the green color channel should thus be dominated by external factors such as ion percolation/mobility. We therefore postulate that NPs with a marked green channel I_f modulation in the +0.03 V to +0.54 V range (subset 2d; also see Figure S7) are characterized by a lower external ion mobility (larger sensitivity to E_{app}) than those that show low modulation within this potential range (subset 2e).

The differential relative amplitude of I_f for the two channels (green vs red) may be rationalized considering the extent of aggregation and energy transfer characterizing green and red emissive sites. Compared to green-emitting sites, red-emitting sites are thought to be better packed and have stronger interchain interactions,[59,60] resulting in better charge transport[22] and faster energy transfer.[19,61] Note that in this context *charge transport* refers to the movement of charge (radical anions or cations) within the conjugated polymer material by means of a hopping mechanism which takes place among nearby chain segments (charge carriers) belonging to the same chain or different chains.[62] Under applied electrochemical potentials we postulate that external ion migration through open spaces in a structure dominated by red-emitting sites is difficult because the corresponding chains are closely packed and have less freedom of motion (Figure 4b).[63] The electric field generated at the working electrode is thus poorly screened for red-emissive sites resulting in a high sensitivity of the associated I_f to changes in E_{app} for a potential window where the only active mechanism is PeT (i.e., marked I_f modulation with E_{app} in the +0.03 V to +0.54 V range, Figures 2 and 5). We further note that the better light harvesting ability of red-emitting over green-emitting sites, due to their intrinsically higher energy transfer efficiency, would lead to a strong amplification of the I_f quenching via excited state redox processes. In other words, the intrinsically longer exciton diffusion length of red-emitting sites results in a higher fraction of excitons reaching the electrode for PeT relative to green-emitting sites. The combined action of poorer external ion mobility (lesser screening) and better energy transfer results in

DOI: 10.1021/acs.jpcc.5b03491
J. Phys. Chem. C 2015, 119, 12875−12886

a stronger relative I_f modulation for red-emitting vs green-emitting sites (Figures 2f, 5d), and is in line with the higher modulation depth recorded for red-emitting sites as previously described (Figure 3). In line with better energy transport, red-emitting sites are more prone to irreversible photodamage following prolonged imaging, as can be observed from the larger relative drop in I_f for red-emitting sites vs green-emitting sites before engaging the applied bias and after disengaging the applied bias (see Figures S5 and S6).

The SMS-EC experiments further reveal a faster (non-hysteretic) response to E_{app} in red- vs green-emitting sites observed as E_{app} are swept to more negative values (up to −0.97 V) (vide infra, see also Figure 5e). This phenomenon could also be explained in terms of better contact between red sites and ITO, and/or higher charge mobility within their characteristically highly aggregated backbone.

Altogether, the above observations reveal that ion mobility, in addition to PPV backbone aggregation, plays a crucial role in determining the interfacial (ITO/MPS-PPV) charge transfer dynamics of the system.

Results for +1.03 V ≥ E_{app} ≥ −0.97 V. Larger I_f enhancements were recorded, in both red and green channels when E_{app} was scanned to negative peak values of −0.97 V (Figure 5). Two differing behaviors were observed at these negative biases. One subset of NPs (∼50% of the total of 76 NPs monitored) displayed a linear response in I_f with E_{app} in the range of +0.54 V to −0.97 V (Figure 5a) while a second subset showed asymmetric I_f response for E_{app} lower than −0.68 V (regions in purple in Figure 5), particularly evident in the green channel (Figure 5b). We draw comparisons between NP subsets 2d and 5a (2e and 5b) that show a higher (lower) sensitivity of I_f to E_{app}. When slowing the potential scan rate by half, to 50 mV/s, all particles showed a single behavior (Figure 5c): specifically, a small change of I_f for potentials between −0.68 V and +0.54 V and a sharp I_f enhancement for E_{app} < −0.68 V. This is the same behavior observed for the subset of particles presented in Figure 5b.

The observed asymmetric behavior at negative bias (purple region in Figure 5) is consistent with the thermal reduction of otherwise nonemissive quenched sites. The reduction potential onset of MPS-PPV is expected to be in the range of −1.3 V to −1.55 V vs NHE by comparison to other 2,5-dialkoxy-substituted PPVs.[49,50] Considering this redox potential and also that the redox process we observed at E_{app} < −0.68 V led to an increase in I_f, as opposed to intensity quenching expected from the formation of MPS-PPV radical anions, we conclude that a species different to pristine MPS-PPV is undergoing reduction at E_{app} more negative than −0.68 V.

We postulate that nonemitting, photooxidized sites along the MPS-PPV backbone were transiently modified under the reductive potentials (< −0.68 V) to nonquenching sites, giving rise to the sharp I_f increase. It is well-known that PPV polymers photooxidize easily resulting in reduced photoluminescence. It is likely that electrochemical reduction of such quenching sites would restore the I_f of the MPS-PPV polymer.[64] Importantly, fluorescence studies on individual MEH-PPV chains suggested that reversible fluorescence restoration is possible at reductive potentials, but only for photooxidized polymer.[65,66] It has been suggested that the photoproducts include species such as dioxetanes or carbonyl defects.[67−71] Carboxylic acids are also thought to be formed during PPV photooxidation.[72] Reversibility of the fluorescence enhancement seen previously,[65] and in this study (in particular Figure 5c, time window 40−60 s) are inconsistent with the irreversible nature of the dissociative reduction of aromatic dioxetanes.[68] Based on the onset potential for the fluorescence enhancement (−0.68 V), aldehyde reduction is unlikely to be the process at play since the reduction potential of an aldehyde-terminated oligo PV was reported to be −2.07 V.[73] On the other hand, the reduction potential of benzoic acid at ∼ −0.7 V vs NHE[74] is in excellent agreement with our observations. It is thus tempting to conclude that carboxylic acid sites are present in the polymer backbone quenching MPS-PPV fluorescence and that they are reversibly reduced at electrode potentials more negative than −0.68 V, restoring the intrinsic polymer fluorescence. A mechanistic overview of the proposed process is detailed in the Supporting Information. Further studies exploring the effect of negative applied biases on the photophysics of (photo-oxidized) MPS-PPV are warranted to elucidate the nature of quenching sites.

Differential ion motion through MPS-PPV NPs, previously invoked to explain the distinct response of the green and red channels toward PeT (vide supra), may also account for the occurrence of electrochemical reduction of a quenching site in only a single subset of NPs at a scan rate of 100 mV/s. Rapid ion motion in response to lowering of the potential (Figure 5b,c) leads to an accumulation of cations at the electrode surface. These cations will stabilize radical anions formed by photoinduced reduction of MPS-PPV and retard the thermodynamically favorable back electron transfer to the ITO (Figure 6). The injected electron will consequently remain

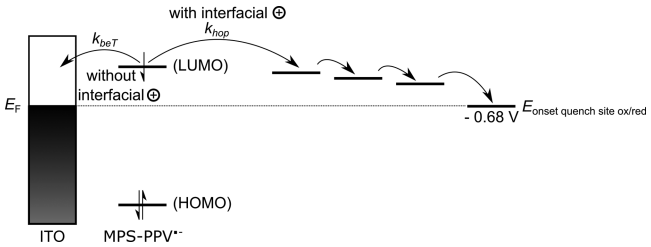

Figure 6. Proposed effect of MPS-PPV/ITO interfacial ions on the electron transport in MPS-PPV NPs. k_{beT} is the rate of back electron transfer from a MPS-PPV radical anion segment (formed upon PeT from ITO to MPS-PPV) to the ITO electrode. k_{hop} is the self-exchange electron transfer rate between MPS-PPV segments, leading to electron mobility in the CPE. The onset energy for reduction of quenching sites is indicated at −0.68 V ($E_{onset\ quench\ site\ ox/red}$) in accordance with experimental observations. Redox potentials for the MPS-PPV$^{\bullet-}$ segment can be roughly approximated to the energy levels of the highest occupied and lowest unoccupied molecular orbitals (HOMO, LUMO) of ground state MPS-PPV.

longer in MPS-PPV, increasing the probability of the electron to be transported away from the electrode through self-exchange reactions (i.e., hopping mechanism), and reduce a quenching site. On the other hand, if cations cannot accumulate to stabilize the initial radical anion formed near the electrode, only a few sites in the NP will be sampled before fast back electron transfer occurs thus lowering the probability of reductively repairing a quenching site. Our view that the differential characteristics between NPs are due to the relative ease of external ion diffusion is further supported by the observation of a higher proportion of aggregated and ordered red-emitting sites, which impede ion diffusion, in the NP subsets associated with slower ion motion (Subsets 2d, 5a; see Figures 2f and 5d).

DOI: 10.1021/acs.jpcc.5b03491
J. Phys. Chem. C 2015, 119, 12875−12886

Focusing next our attention on the recovery of I_f recorded as E_{app} is swept from its peak positive value of +1.03 V toward lower values (e.g., Figure 5a, 35 s and later), we note that I_f is dependent on both the scan rate and the subset of NPs analyzed (see Figure 5f). Previous studies on MEH-PPV NPs have revealed the presence of deep holes (hole traps) upon observation of a slow recovery of I_f following extensive hole injection, similar to our own observations.[26,48,75] As E_{app} decreases from the positive potential peak (+1.03 V), the MPS-PPV fluorescence is restored by filling (electrochemically reducing) holes that were injected in the PPV backbone. We observe a faster recovery of I_f, in other words a faster filling of injected holes, for the subset of NPs depicted in Figure 5b and previously associated with fast external ion migration. Slowing the potential scan rate (subset 5c) results in a larger yield of filled holes at a given bias (i.e., a larger relative intensity restoration at a given bias) consistent with better responsiveness of external ions to changes in E_{app}. There is a positive correlation between the external ion mobility and the charge mobility in the CPE, as previously reported.[45]

Surprisingly, neither the differential rate of recovery of I_f nor the I_f peak response time at E_{app} = +0.03 V were observed when the data was collected in the range between +1.03 V and +0.03 V as shown in Figure 2 (see Figure S9). We attribute the discrepancy when compared to the data with E_{app} reaching −0.97 V to the limiting conditions experienced by the polymer environment; in the latter case, substantial external ion reorganization is expected in response to the relatively large negative bias. The larger changes in E_{app} used for the experiment illustrated in Figure 5 and concomitant ion reorganization directly translate to the optoelectronic properties of MPS-PPV.

In closing, we also considered the effect of particle size on the photophysical properties of the CPE NPs. The optical properties of conjugated polymer NPs mostly depend on the conformation of the polymer and the nature of the aggregates.[28] Size-independent spectroscopic properties have been observed for individual MEH-PPV NPs larger than 10 nm in size.[76] Our SMS-EC experiments performed on NPs originating from the same preparation showed no marked trends in measured properties, e.g., $E_{1/2}$, fluorescence enhancements, and $I_{f\,red}/I_{f\,green}$ (see Figures S10−12), with respect to NP size. Here, the total initial fluorescence intensity of a NP was used as an approximate marker of NP size.[76] Importantly, the changes in spectroscopic properties that parallel changes in size when preparing MPS-PPV NPs in differing water contents (Tables 1 and S1) are attributed to changes in the polymer chain conformation and interchain interactions. We also considered the possibility of surface species playing a role in the heterogeneous fluorescence response to E_{app}. Core−shell structures have been observed for oligomeric phenylenevinylene aggregates where monomer-like chains emitting blue-shifted fluorescence were found on the particle surface.[77,78] In principle, it is possible that the green-emitting sites we observed are preferentially located near the surface of the NPs, yet the small (subdiffraction) size of our particles does not allow us to directly confirm this possibility. Under these conditions, ion migration would be expected to be easier at the NP/solution interface, consistent with our observations of low E_{app} sensitivity for green-emitting sites. However, as mentioned above, we do not observe size-dependent $I_{f\,red}/I_{f\,green}$ ratios to support the localization of green-emitting sites near the surface.

CONCLUSIONS

In summary, we report a simple method for the formation of NPs of the conjugated polyelectrolyte MPS-PPV that exhibit dim and red-shifted fluorescence. The chain conformation of MPS-PPV is greatly influenced by the water content in H_2O/organic solvent mixtures and by the choice of counterion. Tuning the solvent composition enables controlling the emission intensity and color.

The newly prepared CPE NPs revealed heterogeneous fluorescence response to an externally applied potential. The two-color SMS-EC setup used allowed us to spectrally discriminate between deaggregated and aggregated emission sites. The deaggregated coiled MPS-PPV sites, where ion rearrangement is less hindered, were less sensitive to changes in applied bias. We postulate that the reduced sensitivity is a result of better compensation of the effects induced by an applied potential due to higher electrolyte mobility. Quenching sites are present in the CPE, most probably products of photooxidation of polymer segments, and are electrochemically reducible in a reversible fashion which restores the fluorescence of the polymer. When migration of ions through the NP is hindered, charge mobility between CPE segments is slowed down leading to reduced electronic communication between chromophores in the NP and the working electrode and affecting the repair of quenching sites.

Methods that influence CPE chain conformation are highly sought after to tune and improve device applications, where a choice between either high charge mobility or high emission yield is often necessary.[22] Our two-color SMS-EC method herein described provides a tool to explore at the single NP level the interplay between CPE conformation and its optoelectronic properties, distinguishing between poorly and well-packed segments within single MPS-PPV NPs. Our method thus enables evaluation of the effectiveness of protocols that modify polymer chain conformation either in solution or after deposition on a surface.

ASSOCIATED CONTENT

Supporting Information

Particle size distribution from SEM micrograph; spectroscopic data for MPS-PPV NPs dispersed in H_2O/MeCN solutions; additional SMS-EC data and representations; detailed mechanism of fluorescence enhancement under negative applied biases. The Supporting Information is available free of charge on the ACS Publications website at DOI: 10.1021/acs.jpcc.5b03491.

AUTHOR INFORMATION

Corresponding Author

*E-mail: gonzalo.cosa@mcgill.ca.

Notes

The authors declare no competing financial interest.

ACKNOWLEDGMENTS

G.C. is grateful to the Natural Science and Engineering Research Council of Canada (NSERC), a Tomlinson award from McGill University, and the Canadian Foundation for Innovation (CFI) for funding. R.G. is thankful to NSERC for a postgraduate scholarship. This work has been supported in part by grants from the Agencia Nacional de Promoción Científica y Tecnológica (ANPCyT), Argentina (PICT 140/08, 2213/07, 2691/11, and PRH23 PME01); the Consejo Nacional de

DOI: 10.1021/acs.jpcc.5b03491
J. Phys. Chem. C 2015, 119, 12875−12886

Investigaciones Científicas y Técnicas (CONICET), Argentina (PIP 11220090100839/10, 11220100100284/11, and CIAM/09); the Secretaría de Ciencia y Técnica, UNRC Argentina; the Ministerio de Ciencia y Tecnología Cordoba, Argentina (PID 033/2010). R.E.P. is permanent research staff of CONICET.

REFERENCES

(1) Pinto, M. R.; Schanze, K. S. Conjugated Polyelectrolytes: Synthesis and Applications. *Synthesis* **2002**, *2002*, 1293−1309.
(2) Burroughes, J. H.; Bradley, D. D. C.; Brown, A. R.; Marks, R. N.; Mackay, K.; Friend, R. H.; Burns, P. L.; Holmes, A. B. Light-Emitting Diodes Based on Conjugated Polymers. *Nature* **1990**, *347*, 539−541.
(3) Günes, S.; Neugebauer, H.; Sariciftci, N. S. Conjugated Polymer-Based Organic Solar Cells. *Chem. Rev.* **2007**, *107*, 1324−1338.
(4) Hoeben, F. J. M.; Jonkheijm, P.; Meijer, E. W.; Schenning, A. P. H. J. About Supramolecular Assemblies of π-Conjugated Systems. *Chem. Rev.* **2005**, *105*, 1491−1546.
(5) Duarte, A.; Pu, K.-Y.; Liu, B.; Bazan, G. C. Recent Advances in Conjugated Polyelectrolytes for Emerging Optoelectronic Applications. *Chem. Mater.* **2010**, *23*, 501−515.
(6) Chen, H.-Y.; Hou, J.; Zhang, S.; Liang, Y.; Yang, G.; Yang, Y.; Yu, L.; Wu, Y.; Li, G. Polymer Solar Cells with Enhanced Open-Circuit Voltage and Efficiency. *Nat. Photonics* **2009**, *3*, 649−653.
(7) Ha, J. S.; Kim, K. H.; Choi, D. H. 2,5-Bis(2-octyldodecyl)-pyrrolo[3,4-C]pyrrole-1,4-(2H,5H)-dione-Based Donor−Acceptor Alternating Copolymer Bearing 5,5′-di(thiophen-2-yl)-2,2′-biselenophene Exhibiting 1.5 $cm^2 \cdot v^{-1} \cdot s^{-1}$ Hole Mobility in Thin-Film Transistors. *J. Am. Chem. Soc.* **2011**, *133*, 10364−10367.
(8) Thomas, S. W.; Joly, G. D.; Swager, T. M. Chemical Sensors Based on Amplifying Fluorescent Conjugated Polymers. *Chem. Rev.* **2007**, *107*, 1339−1386.
(9) Hu, D.; Yu, J.; Wong, K.; Bagchi, B.; Rossky, P. J.; Barbara, P. F. Collapse of Stiff Conjugated Polymers with Chemical Defects into Ordered, Cylindrical Conformations. *Nature* **2000**, *405*, 1030−1033.
(10) Kim, J.; Swager, T. M. Control of Conformational and Interpolymer Effects in Conjugated Polymers. *Nature* **2001**, *411*, 1030−1034.
(11) Sarzi Sartori, S.; De Feyter, S.; Hofkens, J.; Van der Auweraer, M.; De Schryver, F.; Brunner, K.; Hofstraat, J. W. Host Matrix Dependence on the Photophysical Properties of Individual Conjugated Polymer Chains. *Macromolecules* **2003**, *36*, 500−507.
(12) Ebihara, Y.; Vacha, M. Relating Conformation and Photophysics in Single MEH-PPV Chains. *J. Phys. Chem. B* **2008**, *112*, 12575−12578.
(13) Lupton, J. M. Chromophores in Conjugated Polymers—All Straight? *ChemPhysChem* **2012**, *13*, 901−907.
(14) Botiz, I.; Stingelin, N. Influence of Molecular Conformations and Microstructure on the Optoelectronic Properties of Conjugated Polymers. *Materials* **2014**, *7*, 2273−2300.
(15) Nguyen, T.-Q.; Martini, I. B.; Liu, J.; Schwartz, B. J. Controlling Interchain Interactions in Conjugated Polymers: The Effects of Chain Morphology on Exciton−Exciton Annihilation and Aggregation in MEH-PPV Films. *J. Phys. Chem. B* **2000**, *104*, 237−255.
(16) Kobayashi, H.; Hirata, S.; Vacha, M. Mechanical Manipulation of Photophysical Properties of Single Conjugated Polymer Nanoparticles. *J. Phys. Chem. Lett.* **2013**, *4*, 2591−2596.
(17) Woll, D.; Braeken, E.; Deres, A.; De Schryver, F. C.; Uji-i, H.; Hofkens, J. Polymers and Single Molecule Fluorescence Spectroscopy, What Can We Learn? *Chem. Soc. Rev.* **2009**, *38*, 313−328.
(18) Schwartz, B. J. Conjugated Polymers as Molecular Materials: How Chain Conformation and Film Morphology Influence Energy Transfer and Interchain Interactions. *Annu. Rev. Phys. Chem.* **2003**, *54*, 141−172.
(19) Nguyen, T.-Q.; Wu, J.; Doan, V.; Schwartz, B. J.; Tolbert, S. H. Control of Energy Transfer in Oriented Conjugated Polymer-Mesoporous Silica Composites. *Science* **2000**, *288*, 652−656.
(20) Hu, Z.; Adachi, T.; Haws, R.; Shuang, B.; Ono, R. J.; Bielawski, C. W.; Landes, C. F.; Rossky, P. J.; Vanden Bout, D. A. Excitonic Energy Migration in Conjugated Polymers: The Critical Role of Interchain Morphology. *J. Am. Chem. Soc.* **2014**, *136*, 16023−16031.
(21) Hwang, I.; Scholes, G. D. Electronic Energy Transfer and Quantum-Coherence in π-Conjugated Polymers. *Chem. Mater.* **2011**, *23*, 610−620.
(22) Garcia, A.; Nguyen, T.-Q. Effect of Aggregation on the Optical and Charge Transport Properties of an Anionic Conjugated Polyelectrolyte. *J. Phys. Chem. C* **2008**, *112*, 7054−7061.
(23) Wang, D.; Lal, J.; Moses, D.; Bazan, G. C.; Heeger, A. J. Small Angle Neutron Scattering (SANS) Studies of a Conjugated Polyelectrolyte in Aqueous Solution. *Chem. Phys. Lett.* **2001**, *348*, 411−415.
(24) Gao, Y.; Wang, C.-C.; Wang, L.; Wang, H.-L. Conjugated Polyelectrolytes with Ph-Dependent Conformations and Optical Properties. *Langmuir* **2007**, *23*, 7760−7767.
(25) Schnablegger, H.; Antonietti, M.; Göltner, C.; Hartmann, J.; Cölfen, H.; Samori, P.; Rabe, J. P.; Häger, H.; Heitz, W. Morphological Characterization of the Molecular Superstructure of Polyphenylene Ethynylene Derivatives. *J. Colloid Interface Sci.* **1999**, *212*, 24−32.
(26) Palacios, R. E.; Fan, F.-R. F.; Grey, J. K.; Suk, J.; Bard, A. J.; Barbara, P. F. Charging and Discharging of Single Conjugated-Polymer Nanoparticles. *Nat. Mater.* **2007**, *6*, 680−685.
(27) Szymanski, C.; Wu, C.; Hooper, J.; Salazar, M. A.; Perdomo, A.; Dukes, A.; McNeill, J. Single Molecule Nanoparticles of the Conjugated Polymer MEH-PPV, Preparation and Characterization by near-Field Scanning Optical Microscopy. *J. Phys. Chem. B* **2005**, *109*, 8543−8546.
(28) Tuncel, D.; Demir, H. V. Conjugated Polymer Nanoparticles. *Nanoscale* **2010**, *2*, 484−494.
(29) Pecher, J.; Mecking, S. Nanoparticles of Conjugated Polymers. *Chem. Rev.* **2010**, *110*, 6260−6279.
(30) Wu, C.; Chiu, D. T. Highly Fluorescent Semiconducting Polymer Dots for Biology and Medicine. *Angew. Chem., Int. Ed.* **2013**, *52*, 3086−3109.
(31) Bustamante, C.; Maestre, M. F. Statistical Effects in the Absorption and Optical Activity of Particulate Suspensions. *Proc. Natl. Acad. Sci. U. S. A.* **1988**, *85*, 8482−8486.
(32) Choi, J.; Ruiz, C. R.; Nesterov, E. E. Temperature-Induced Control of Conformation and Conjugation Length in Water-Soluble Fluorescent Polythiophenes. *Macromolecules* **2010**, *43*, 1964−1974.
(33) Tretiak, S.; Saxena, A.; Martin, R. L.; Bishop, A. R. Interchain Electronic Excitations in Poly(phenylenevinylene) (PPV) Aggregates. *J. Phys. Chem. B* **2000**, *104*, 7029−7037.
(34) Pinto, M. R.; Kristal, B. M.; Schanze, K. S. A Water-Soluble Poly(phenylene Ethynylene) with Pendant Phosphonate Groups. Synthesis, Photophysics, and Layer-by-Layer Self-Assembled Films. *Langmuir* **2003**, *19*, 6523−6533.
(35) Traiphol, R.; Charoenthai, N.; Srikhirin, T.; Kerdcharoen, T.; Osotchan, T.; Maturos, T. Chain Organization and Photophysics of Conjugated Polymer in Poor Solvents: Aggregates, Agglomerates and Collapsed Coils. *Polymer* **2007**, *48*, 813−826.
(36) Wang, M.; Zou, S.; Guerin, G.; Shen, L.; Deng, K.; Jones, M.; Walker, G. C.; Scholes, G. D.; Winnik, M. A.; Water-Soluble Ph-Responsive, A. Molecular Brush of Poly(N,N-dimethylaminoethyl Methacrylate) Grafted Polythiophene. *Macromolecules* **2008**, *41*, 6993−7002.
(37) Feist, F. A.; Zickler, M. F.; Basché, T. Origin of the Red Sites and Energy Transfer Rates in Single MEH-PPV Chains at Low Temperature. *ChemPhysChem* **2011**, *12*, 1499−1508.
(38) Potai, R.; Traiphol, R. Controlling Chain Organization and Photophysical Properties of Conjugated Polymer Nanoparticles Prepared by Reprecipitation Method: The Effect of Initial Solvent. *J. Colloid Interface Sci.* **2013**, *403*, 58−66.
(39) Lemmer, U.; Heun, S.; Mahrt, R. F.; Scherf, U.; Hopmeier, M.; Siegner, U.; Göbel, E. O.; Müllen, K.; Bässler, H. Aggregate Fluorescence in Conjugated Polymers. *Chem. Phys. Lett.* **1995**, *240*, 373−378.
(40) Aryanpour, K.; Sheng, C. X.; Olejnik, E.; Pandit, B.; Psiachos, D.; Mazumdar, S.; Vardeny, Z. V. Evidence for Excimer Photo-

DOI: 10.1021/acs.jpcc.5b03491
J. Phys. Chem. C 2015, 119, 12875−12886

excitations in an Ordered π-Conjugated Polymer Film. *Phys. Rev. B* **2011**, *83*, 155124.
(41) Smith, A.; Shen, C.-F.; Roberts, S.; Helgeson, R.; Schwartz, B. Ionic Strength and Solvent Control over the Physical Structure, Electronic Properties and Superquenching of Conjugated Polyelectrolytes. *Res. Chem. Intermed.* **2007**, *33*, 125−142.
(42) Jakubiak, R.; Collison, C. J.; Wan, W. C.; Rothberg, L. J.; Hsieh, B. R. Aggregation Quenching of Luminescence in Electroluminescent Conjugated Polymers. *J. Phys. Chem. A* **1999**, *103*, 2394−2398.
(43) Collini, E.; Scholes, G. D. Coherent Intrachain Energy Migration in a Conjugated Polymer at Room Temperature. *Science* **2009**, *323*, 369−373.
(44) Hoven, C. V.; Garcia, A.; Bazan, G. C.; Nguyen, T.-Q. Recent Applications of Conjugated Polyelectrolytes in Optoelectronic Devices. *Adv. Mater.* **2008**, *20*, 3793−3810.
(45) Yang, R.; Garcia, A.; Korystov, D.; Mikhailovsky, A.; Bazan, G. C.; Nguyen, T.-Q. Control of Interchain Contacts, Solid-State Fluorescence Quantum Yield, and Charge Transport of Cationic Conjugated Polyelectrolytes by Choice of Anion. *J. Am. Chem. Soc.* **2006**, *128*, 16532−16539.
(46) Palacios, R. E.; Fan, F.-R. F.; Bard, A. J.; Barbara, P. F. Single-Molecule Spectroelectrochemistry (SMS-EC. *J. Am. Chem. Soc.* **2006**, *128*, 9028−9029.
(47) Bard, A. J.; Faulkner, L. R. *Electrochemical Methods: Fundamentals and Applications*, 2nd ed.; Wiley: Hoboken, 2001.
(48) Palacios, R. E.; Chang, W.-S.; Grey, J. K.; Chang, Y.-L.; Miller, W. L.; Lu, C.-Y.; Henkelman, G.; Zepeda, D.; Ferraris, J.; Barbara, P. F. Detailed Single-Molecule Spectroelectrochemical Studies of the Oxidation of Conjugated Polymers. *J. Phys. Chem. B* **2009**, *113*, 14619−14628.
(49) Li, Y.; Cao, Y.; Gao, J.; Wang, D.; Yu, G.; Heeger, A. J. Electrochemical Properties of Luminescent Polymers and Polymer Light-Emitting Electrochemical Cells. *Synth. Met.* **1999**, *99*, 243−248.
(50) Holt, A. L.; Leger, J. M.; Carter, S. A. Electrochemical and Optical Characterization of P- and N-Doped Poly[2-methoxy-5-(2-ethylhexyloxy)-1,4-phenylenevinylene]. *J. Chem. Phys.* **2005**, *123*, 044704 1−7.
(51) Deussen, M.; Scheidler, M.; Bässler, H. Electric Field-Induced Photoluminescence Quenching in Thin-Film Light-Emitting Diodes Based on Poly(phenyl-p-phenylene Vinylene). *Synth. Met.* **1995**, *73*, 123−129.
(52) Smith, T. M.; Hazelton, N.; Peteanu, L. A.; Wildeman, J. Electrofluorescence of MEH-PPV and Its Oligomers: Evidence for Field-Induced Fluorescence Quenching of Single Chains. *J. Phys. Chem. B* **2006**, *110*, 7732−7742.
(53) Moscatelli, A.; Livingston, K.; So, W. Y.; Lee, S. J.; Scherf, U.; Wildeman, J.; Peteanu, L. A. Electric-Field-Induced Fluorescence Quenching in Polyfluorene, Ladder-Type Polymers, and MEH-PPV: Evidence for Field Effects on Internal Conversion Rates in the Low Concentration Limit. *J. Phys. Chem. B* **2010**, *114*, 14430−14439.
(54) Heinze, J.; Tschuncky, P. Electrochemical Properties. In *Electronic Materials: The Oligomer Approach*; Wiley-VCH Verlag GmbH: Weinheim, 1998; pp 479−514.
(55) Wu, H.; Huang, F.; Mo, Y.; Yang, W.; Wang, D.; Peng, J.; Cao, Y. Efficient Electron Injection from a Bilayer Cathode Consisting of Aluminum and Alcohol-/Water-Soluble Conjugated Polymers. *Adv. Mater.* **2004**, *16*, 1826−1830.
(56) Wu, H.; Huang, F.; Peng, J.; Cao, Y. High-Efficiency Electron Injection Cathode of Au for Polymer Light-Emitting Devices. *Org. Electron.* **2005**, *6*, 118−128.
(57) Ishii, H.; Sugiyama, K.; Ito, E.; Seki, K. Energy Level Alignment and Interfacial Electronic Structures at Organic/Metal and Organic/Organic Interfaces. *Adv. Mater.* **1999**, *11*, 605−625.
(58) Hoven, C. V.; Peet, J.; Mikhailovsky, A.; Nguyen, T.-Q. Direct Measurement of Electric Field Screening in Light Emitting Diodes with Conjugated Polyelectrolyte Electron Injecting/Transport Layers. *Appl. Phys. Lett.* **2009**, *94*, 033301 1−3.
(59) Nguyen, T.-Q.; Schwartz, B. J.; Schaller, R. D.; Johnson, J. C.; Lee, L. F.; Haber, L. H.; Saykally, R. J. Near-Field Scanning Optical Microscopy (NSOM) Studies of the Relationship between Interchain Interactions, Morphology, Photodamage, and Energy Transport in Conjugated Polymer Films. *J. Phys. Chem. B* **2001**, *105*, 5153−5160.
(60) Schaller, R. D.; Snee, P. T.; Johnson, J. C.; Lee, L. F.; Wilson, K. R.; Haber, L. H.; Saykally, R. J.; Nguyen, T.-Q.; Schwartz, B. J. Nanoscopic Interchain Aggregate Domain Formation in Conjugated Polymer Films Studied by Third Harmonic Generation near-Field Scanning Optical Microscopy. *J. Chem. Phys.* **2002**, *117*, 6688−6698.
(61) Nguyen, T. Q.; Wu, J.; Tolbert, S. H.; Schwartz, B. J. Control of Energy Transport in Conjugated Polymers Using an Ordered Mesoporous Silica Matrix. *Adv. Mater.* **2001**, *13*, 609−611.
(62) Heeger, A. J.; Kivelson, S.; Schrieffer, J. R.; Su, W. P. Solitons in Conducting Polymers. *Rev. Mod. Phys.* **1988**, *60*, 781−850.
(63) Garcia, A.; Bakus, R. C., II; Zalar, P.; Hoven, C. V.; Brzezinski, J. Z.; Nguyen, T.-Q. Controlling Ion Motion in Polymer Light-Emitting Diodes Containing Conjugated Polyelectrolyte Electron Injection Layers. *J. Am. Chem. Soc.* **2011**, *133*, 2492−2498.
(64) Liu, H.-W.; Ngo, A. T.; Cosa, G. Enhancing the Emissive Properties of Poly(p-phenylenevinylene)-Conjugated Polyelectrolyte-Coated SiO_2 Nanoparticles. *J. Am. Chem. Soc.* **2011**, *134*, 1648−1652.
(65) Park, S.-J.; Gesquiere, A. J.; Yu, J.; Barbara, P. F. Charge Injection and Photooxidation of Single Conjugated Polymer Molecules. *J. Am. Chem. Soc.* **2004**, *126*, 4116−4117.
(66) Gesquiere, A. J.; Park, S.-J.; Barbara, P. F. F−V/SMS: A New Technique for Studying the Structure and Dynamics of Single Molecules and Nanoparticles. *J. Phys. Chem. B* **2004**, *108*, 10301−10308.
(67) Cornil, J.; dos Santos, D. A.; Crispin, X.; Silbey, R.; Brédas, J. L. Influence of Interchain Interactions on the Absorption and Luminescence of Conjugated Oligomers and Polymers: A Quantum-Chemical Characterization. *J. Am. Chem. Soc.* **1998**, *120*, 1289−1299.
(68) Stringle, D. L. B.; Nevin Campbell, R.; Workentin, M. S. Radical Anion Chain Process Initiated by a Dissociative Electron Transfer to a Monocyclic Endoperoxide. *Chem. Commun.* **2003**, 1246−1247.
(69) Scurlock, R. D.; Wang, B.; Ogilby, P. R.; Sheats, J. R.; Clough, R. L. Singlet Oxygen as a Reactive Intermediate in the Photodegradation of an Electroluminescent Polymer. *J. Am. Chem. Soc.* **1995**, *117*, 10194−10202.
(70) Dam, N.; Scurlock, R. D.; Wang, B.; Ma, L.; Sundahl, M.; Ogilby, P. R. Singlet Oxygen as a Reactive Intermediate in the Photodegradation of Phenylenevinylene Oligomers. *Chem. Mater.* **1999**, *11*, 1302−1305.
(71) Burrows, H. D.; Narwark, O.; Peetz, R.; Thorn-Csanyi, E.; Monkman, A. P.; Hamblett, I.; Navaratnam, S. Mechanistic Studies on the Photodegradation of 2,5-Dialkyloxyl-Substituted para-Phenylenevinylene Oligomers by Singlet Oxygen. *Photochem. Photobiol. Sci.* **2010**, *9*, 942−948.
(72) Chambon, S.; Rivaton, A.; Gardette, J.-L.; Firon, M. Photo- and Thermo-Oxidation of Poly(p-phenylene-vinylene) and Phenylene-Vinylene Oligomer. *Polym. Degrad. Stab.* **2011**, *96*, 1149−1158.
(73) Guerlin, A.; Dumur, F.; Dumas, E.; Miomandre, F.; Wantz, G.; Mayer, C. R. Tunable Optical Properties of Chromophores Derived from Oligo(p-phenylene Vinylene). *Org. Lett.* **2010**, *12*, 2382−2385.
(74) Silvester, D. S.; He, W.; Aldous, L.; Hardacre, C.; Compton, R. G. Electrochemical Reduction of Benzoic Acid and Substituted Benzoic Acids in Some Room Temperature Ionic Liquids. *J. Phys. Chem. C* **2008**, *112*, 12966−12973.
(75) Bolinger, J. C.; Fradkin, L.; Lee, K.-J.; Palacios, R. E.; Barbara, P. F. Light-Assisted Deep-Trapping of Holes in Conjugated Polymers. *Proc. Natl. Acad. Sci. U. S. A.* **2009**, *106*, 1342−1346.
(76) Grey, J. K.; Kim, D. Y.; Norris, B. C.; Miller, W. L.; Barbara, P. F. Size-Dependent Spectroscopic Properties of Conjugated Polymer Nanoparticles. *J. Phys. Chem. B* **2006**, *110*, 25568−25572.
(77) Peteanu, L. A.; Sherwood, G. A.; Werner, J. H.; Shreve, A. P.; Smith, T. M.; Wildeman, J. Visualizing Core−Shell Structure in Substituted PPV Oligomer Aggregates Using Fluorescence Lifetime Imaging Microscopy (FLIM). *J. Phys. Chem. C* **2011**, *115*, 15607−15616.

DOI: 10.1021/acs.jpcc.5b03491
J. Phys. Chem. C 2015, 119, 12875−12886

(78) So, W. Y.; Hong, J.; Kim, J. J.; Sherwood, G. A.; Chacon-Madrid, K.; Werner, J. H.; Shreve, A. P.; Peteanu, L. A.; Wildeman, J. Effects of Solvent Properties on the Spectroscopy and Dynamics of Alkoxy-Substituted PPV Oligomer Aggregates. *J. Phys. Chem. B* **2012**, *116*, 10504−10513.

DOI: 10.1021/acs.jpcc.5b03491
J. Phys. Chem. C 2015, 119, 12875−12886